Journal of Sound and Vibration (1997) **203**(3), 409–434

ACTIVE CONTROL OF VIBRATION TRANSMISSION IN A CYLINDRICAL SHELL

X. PAN AND C. H. HANSEN

Department of Mechanical Engineering, University of Adelaide, Adelaide, SA 5005, *Australia*

(*Received* 11 *July* 1995, *and in final form* 30 *September* 1996)

The theoretical analysis of active control of harmonic power transmission in a semi-infinite cylinder using a circumferential array of control forces and a circumferential array of error sensors is considered, and the extent of control which is achievable for a realistic control force configuration is examined.

The model considered is a semi-infinite cylinder, simply supported at one end, anechoically terminated at the other end and excited harmonically by an array of in-phase primary forces arranged in a line around its circumference. Control is achieved by an array of independent control forces applied downstream from the primary forces. For three or more control forces it is possible to achieve a power transmission reduction of 30 dB for both acceleration and power transmission cost functions, provided that the error sensors are in the far field of the primary and control forces.

1. INTRODUCTION

Active control of structural vibration is a topic which has received considerable attention in the past and will continue to do so in the future as faster and cheaper electronic hardware becomes available to implement control configurations. Active control has been used in the past for minimizing vibration transmission in (one-dimensional) beams and (two-dimensional) plates. Pan and Hansen have studied active control of vibratory power transmission in an infinite beam [1], active control of vibration amplitude in a finite beam [2] and active control of vibratory power transmission in an infinite plate [3, 4].

Flügge [5] described the three-dimensional equations of motion for the vibration of a cylindrical shell. Leissa [6] carried out a numerical analysis which showed that similar results were obtained by the use of Flügge's equations, and the equations of various authors including Forsberg [7, 8]. Subsequently, Flügge has been recognized as the pre-eminent author in this field. However, little research has been carried out to test the validity of Flügge's equations in practical active vibration control applications. In particular, it should be noted that Flügge's model includes a simplifying assumption which does not take into account the linear inertia of the cylinder, and the assumption can cause inaccurate results. Thus, Flügge's model could not be used directly for the active control applications addressed in this paper. It was necessary to develop a more fundamental approach to the model, taking account of cylinder inertia. The extension of Flügge's equations with the inertia terms included, is considered in this paper.

Recently, attention has been given to the feedforward active control of noise in a cylinder which represents an aircraft fuselage. However, the research is mainly directed at reducing the noise radiated from a cylindrical shell or transmitted through it rather than reducing

0022–460X/97/230409 + 26 $25.00/0/sv960787

vibratory power transmission along it. Fuller and Jones [9] presented an experimental investigation on the control of interior noise in a cylinder using a single point vibration control source to reduce noise transmission. Jones and Fuller [10] extended this work to include more control sources. They showed that significant reduction can be achieved for harmonic excitation. Elliott *et al*. [11] demonstrated successful experiments on the control of the noise field in a cabin of an aircraft, by using acoustic rather than vibration control sources.

Feedforward active control of vibratory power transmission in a pipe, i.e., a cylinder with small diameter, has been the subject of increasing attention in recent years. Fuller and Brevart [12] demonstrated the active control of vibratory power transmission in a pipe by using point control sources to minimize the acceleration of the shell around its circumference at several axial locations. However, they considered mainly the low frequency range (well below the ring frequency) where, based on earlier work by Pinnington and Briscoe [13], the pipe behaves as a beam. Their method may be difficult to apply to a cylinder with a large diameter and over a wide frequency range.

Examining the control of vibratory power transmission along a semi-infinite cylinder is one step along the path towards the development of an active system to control vibratory power transmission in large cylindrical structures, where the amplitude of the wave reflected from at least one of the boundaries is negligible compared to that of the original incident wave.

The work outlined here examines the extent of control of flexural, extensional and torsional waves which is achievable for a circumferential array of radial control forces on a semi-infinite cylinder. The cylinder is simply supported at one end, anechoically terminated at the other end and excited by an array of in-phase harmonic primary radial forces arranged in a line around its circumference. The total power transmission reduction is calculated for different wave type acceleration and different wave type power transmission cost functions. In addition, the effect of error sensor type and location, control force type and location, cylinder thickness, radius and excitation frequency is investigated and discussed in detail. As it is difficult to measure power transmission in practice, it is of interest to examine theoretically the effectiveness of minimizing acceleration at the error sensors to reduce power transmission. This is done for a number of error sensor configurations.

2. ACTIVE CONTROL OF ACCELERATION

For active control of structural vibration, the two fundamental approaches are acceleration control and power transmission control. The former is considered in this section, while the latter is discussed in section 4.

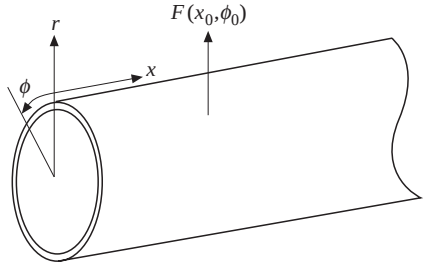

Figure 1. A cylinder with excitation F at location (x_0, ϕ_0).

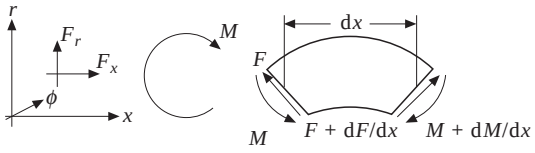

Figure 2. Sign conventionns for forces and moments (conventions for forces and moments in the ϕ-plane are similar).

The geometry of the cylinder and co-ordinates are shown in Figure 1, and the sign conventions are shown in Figure 2. The analysis described here is based on point forces and sensors, which can be approximated very well by using electrodynamic shakers and accelerometers [14]. It should be noted that strain sensors and actuators can also be applied using a similar but modified analysis to that described in this paper [15, 16].

2.1. MINIMIZATION OF ACCELERATION WITH A LINE OF IN-PHASE CONTROL FORCES

If the cylinder is excited by an array of in-phase radial primary forces of complex amplitude F_p located at $x = x_p$, the flexural displacement $w(x, \phi)$ at any location (x, ϕ) is discussed in Appendix A and is found by using equation (A48) in Appendix A as follows:

$$w(x, \phi) = F_p w_{p-f}(x, \phi). \tag{1}$$

Similarly, if an array of radial control forces of complex amplitude F_c are placed at $x = x_c$, the flexural displacement due to this acting alone is

$$w(x, \phi) = F_c w_{c-f}(x, \phi). \tag{2}$$

The total flexural displacement response at location (x, ϕ) due to the primary and control forces acting together is then

$$w(x, \phi) = F_p w_{p-f}(x, \phi) + F_c w_{c-f}(x, \phi). \tag{3}$$

The optimal control force F_c for minimizing the flexural acceleration (and the flexural displacement for a single excitation frequency) around the circumference of the cylinder at a constant axial location x may be found by integrating the sum of the squares of the flexural displacement defined in equation (3) around the circumference of the cylinder, and setting the partial derivatives of the integration with respect to the real and imaginary components of the control force equal to zero. The partial derivatives are

$$\frac{\partial \int_0^{2\pi} |w|^2 \, d\phi}{\partial F_{rel}} = \int_0^{2\pi} (F_p w_{p-f} w_{c-f}^* + F_p^* w_{p-f}^* w_{c-f} + 2F_{rel}|w_{c-f}|^2) \, d\phi \tag{4}$$

and

$$\frac{\partial \int_0^{2\pi} |w|^2 \, d\phi}{\partial F_{img}} = \int_0^{2\pi} (-jF_p w_{p-f} w_{c-f}^* + jF_p w_{p-f}^* w_{c-f} + 2F_{img}|w_{c-f}|^2) \, d\phi \tag{5}$$

respectively, where $F_c = F_{rel} + jF_{img}$ and the superscript asterisk represents the complex conjugate. The physical significance of equations (4) and (5) is that the minimum in the

displacement as a function of the real and imaginary parts of the force occurs when the slope of the function is zero. The result is

$$F_c = -F_p \frac{\int_0^{2\pi} w_{p-f} w_{c-f}^* \, \mathrm{d}\phi}{\int_0^{2\pi} |w_{c-f}|^2 \, \mathrm{d}\phi}. \tag{6}$$

The axial and circumferential displacement due to the radial primary and radial control forces are

$$u(x, \phi) = F_p u_{p-f}(x, \phi) + F_c u_{c-f}(x, \phi) \tag{7}$$

and

$$v(x, \phi) = F_p v_{p-f}(x, \phi) + F_c v_{c-f}(x, \phi) \tag{8}$$

respectively.

2.2. MINIMIZATION OF ACCELERATION WITH A LINE OF THREE INDEPENDENTLY DRIVEN CONTROL FORCES

If the cylinder is driven by an array of in-phase radial primary point forces around one circumference of the cylinder at $x = x_p$ and three independent radial control point forces around the other circumference at $x = x_c$, the total radial displacement response may be written as

$$w = w_p + w_c = F_p w_{p-f} + F_{c1} w_{c-f1} + F_{c2} w_{c-f2} + F_{c3} w_{c-f3}. \tag{9}$$

The quantities w_{c-f1}, w_{c-f2} and w_{c-f3} are each calculated in a similar way to w_{c-f} in Appendix A. The optimal control forces for minimizing the flexural acceleration or displacement at any axial location x may be found by integrating the sum of the squares of the flexural displacement defined in equation (9) around the circumference of the cylinder and setting the partial derivatives of the integration with respect to each of the real and imaginary components of the control forces equal to zero. The result is an optimal set of control forces as follows:

$$\begin{bmatrix} F_{c1} \\ F_{c2} \\ F_{c3} \end{bmatrix} = - \begin{bmatrix} \int_0^{2\pi} |w_{c-f1}|^2 \, \mathrm{d}\phi & \int_0^{2\pi} w_{c-f1}^* w_{c-f2} \, \mathrm{d}\phi & \int_0^{2\pi} w_{c-f1}^* w_{c-f3} \, \mathrm{d}\phi \\ \int_0^{2\pi} w_{c-f1} w_{c-f2}^* \, \mathrm{d}\phi & \int_0^{2\pi} |w_{c-f2}|^2 \, \mathrm{d}\phi & \int_0^{2\pi} w_{c-f2}^* w_{c-f3} \, \mathrm{d}\phi \\ \int_0^{2\pi} w_{c-f1} w_{c-f3}^* \, \mathrm{d}\phi & \int_0^{2\pi} w_{c-f2} w_{c-f3}^* \, \mathrm{d}\phi & \int_0^{2\pi} |w_{c-f3}|^2 \, \mathrm{d}\phi \end{bmatrix}^{-1}$$

$$\times \begin{bmatrix} \int_0^{2\pi} w_{p-f} w_{c-f1}^* \, \mathrm{d}\phi \\ \int_0^{2\pi} w_{p-f} w_{c-f2}^* \, \mathrm{d}\phi \\ \int_0^{2\pi} w_{p-f} w_{c-f3}^* \, \mathrm{d}\phi \end{bmatrix} F_p. \tag{10}$$

The procedure can be extended to any number of independently controlled forces.

3. POWER TRANSMISSION PAST THE ERROR SENSORS

The vibratory power transmission is a result of three wave motions, and is given by Fuller [17], as

$$P_s = P_f + P_e + P_t, \tag{11}$$

where the subscript refers to the shell motion; i.e., either flexure, extension or torsion respectively. The quantity P_f consists of two parts contributed by rotation of the cylindrical element as well as radial flexure. Thus

$$P_f = \frac{1}{T} \int_0^T \int_0^{2\pi} \left[M_x \frac{\partial \theta_x}{\partial t} + Q_x \frac{\partial w}{\partial t} \right] r \, \mathrm{d}\phi \, \mathrm{d}t, \tag{12}$$

$$P_e = \frac{1}{T} \int_0^T \int_0^{2\pi} N_x \frac{\partial u}{\partial t} r \, \mathrm{d}\phi \, \mathrm{d}t \tag{13}$$

and

$$P_t = \frac{1}{T} \int_0^T \int_0^{2\pi} N_{x\phi} \frac{\partial v}{\partial t} r \, \mathrm{d}\phi \, \mathrm{d}t, \tag{14}$$

where T is the period of vibration and θ_x is angular rotation of the cylindrical element about the ϕ-axis. Substituting equations (12), (13) and (14) into equation (11), equation (11) can be written as

$$P_s = \frac{1}{T} \int_0^T \int_0^{2\pi} \left[M_x \frac{\partial \theta_x}{\partial t} + Q_x \frac{\partial w}{\partial t} + N_x \frac{\partial u}{\partial t} + N_{x\phi} \frac{\partial v}{\partial t} \right] r \, \mathrm{d}\phi \, \mathrm{d}t. \tag{15}$$

Adopting the approach of Skudrzyk [18], the real (or active) part of the power transmission along the cylinder for harmonic excitation is calculated as the product of the real part of the force term with the real part of the velocity term for each pair of terms in equation (15) and the result is time averaged. Thus the active power transmission is given by

$$P_s = \frac{r}{2} \int_0^{2\pi} \mathrm{Re} \left[M_x \frac{\partial \theta_x^*}{\partial t} + Q_x \frac{\partial w^*}{\partial t} + N_x \frac{\partial u^*}{\partial t} + N_{x\phi} \frac{\partial v^*}{\partial t} \right] \mathrm{d}\phi \tag{16}$$

where, according to Flügge [5], the bending moment about the ϕ-axis is as shown in equation (A26), the axial force is given by

$$N_x = \frac{D_e}{r}(u' + vv^{\cdot} + vw) - \frac{K}{r^3}w'', \tag{17}$$

where $D_e = Eh/(1 - v^2)$, and $K = Eh^3/[12(1 - v^2)]$, the circumferential shear force is given by

$$N_{x\phi} = \frac{D_e}{r}\frac{1 - v}{2}(u^{\cdot} + v') + \frac{K}{r^3}\frac{1 - v}{2}(v' - w'^{\cdot}) \tag{18}$$

and the transverse shear force is given by

$$Q_x = \frac{K}{r^3}[(w''' + vw'^{\cdot\cdot} - u'' - vv'^{\cdot}) + (1 - v)(w'^{\cdot\cdot} + \tfrac{1}{2}u^{\cdot\cdot} - \tfrac{1}{2}v'^{\cdot})]. \tag{19}$$

For one line of primary actuators around one circumference of the cylinder and a second line of control actuators around the other, the resulting total power transmission along the cylinder can be expressed in terms of the primary and control forces, using superposition. Thus the power transmission corresponding to equation (6) (representing optimal control of flexural acceleration) is obtained by substituting equation (6) into equations (3), (7) and (8), then into equations (A26) and (17)–(19), and the results into equation (16). The power transmission corresponding to equation (10) can be obtained in a similar way.

4. ACTIVE CONTROL OF VIBRATORY POWER TRANSMISSION

4.1. MINIMIZATION OF POWER TRANSMISSION WITH A LINE OF IN-PHASE POINT CONTROL FORCES

The power transmission resulting from a line of in-phase radial primary forces and a line of in-phase radial control forces acting together can be found by substituting equations (3), (7) and (8) into (A26) and (17)–(19) and the results into equation (16). Carrying out the indicated substitutions in equations (A26) and (17)–(19) gives the following expressions for the bending moment, axial force, circumferential force and transverse shear force respectively.

$$M_x = \frac{K}{r^2}\left[\left(F_p\frac{\partial^2 w_{p-f}}{\partial x^2} + F_c\frac{\partial^2 w_{c-f}}{\partial x^2}\right) + v\left(F_p\frac{\partial^2 w_{p-f}}{\partial \phi^2} + F_c\frac{\partial^2 w_{c-f}}{\partial \phi^2}\right)\right.$$

$$\left. - \left(F_p\frac{\partial u_{p-f}}{\partial x} + F_c\frac{\partial u_{c-f}}{\partial x}\right) - v\left(F_p\frac{\partial v_{p-f}}{\partial \phi} + F_c\frac{\partial v_{c-f}}{\partial \phi}\right)\right], \tag{20}$$

$$N_x = \frac{D_e}{r}\left[\left(F_p\frac{\partial u_{p-f}}{\partial x} + F_c\frac{\partial u_{c-f}}{\partial x}\right) + v\left(F_p\frac{\partial v_{p-f}}{\partial \phi} + F_c\frac{\partial v_{c-f}}{\partial \phi}\right)\right.$$

$$\left. + v(F_p w_{p-f} + F_c w_{c-f})\right] - \frac{K}{r^3}\left(F_p\frac{\partial^2 w_{p-f}}{\partial x^2} + F_c\frac{\partial^2 w_{c-f}}{\partial x^2}\right), \tag{21}$$

$$N_{x\phi} = \frac{D_e}{r}\frac{1 - v}{2}\left[\left(F_p\frac{\partial u_{p-f}}{\partial \phi} + F_c\frac{\partial u_{c-f}}{\partial \phi}\right) + \left(F_p\frac{\partial v_{p-f}}{\partial x} + F_c\frac{\partial v_{c-f}}{\partial x}\right)\right.$$

$$\times \frac{K}{r^3}\frac{1-\nu}{2}\left[\left(F_p\frac{\partial v_{p-f}}{\partial x}+F_c\frac{\partial v_{c-f}}{\partial x}\right)-\left(F_p\frac{\partial^2 w_{p-f}}{\partial x\partial\phi}+F_c\frac{\partial^2 w_{c-f}}{\partial x\partial\phi}\right]\right. \tag{22}$$

and

$$\begin{aligned}Q_x=\frac{K}{r^3}\left\{\left[\left(F_p\frac{\partial^3 w_{p-f}}{\partial x^3}+F_c\frac{\partial^3 w_{c-f}}{\partial x^3}\right)+\nu\left(F_p\frac{\partial^3 w_{p-f}}{\partial x\,\partial\phi^2}+F_c\frac{\partial^3 w_{c-f}}{\partial x\,\partial\phi^2}\right)\right.\right.\\ \left.-\left(F_p\frac{\partial^2 u_{p-f}}{\partial x^2}+F_c\frac{\partial^2 u_{c-f}}{\partial x^2}\right)-\nu\left(F_p\frac{\partial^2 v_{p-f}}{\partial x\,\partial\phi}+F_c\frac{\partial^2 v_{c-f}}{\partial x\,\partial\phi}\right)\right]\\ +(1-\nu)\left[\left(F_p\frac{\partial^3 w_{p-f}}{\partial x\,\partial\phi^2}+F_c\frac{\partial^3 w_{c-f}}{\partial x\,\partial\phi^2}\right)+\frac{1}{2}\left(F_p\frac{\partial^2 u_{p-f}}{\partial\phi^2}+F_c\frac{\partial^2 u_{c-f}}{\partial\phi^2}\right)\right.\\ \left.\left.\left.-\frac{1}{2}\left(F_p\frac{\partial^2 v_{p-f}}{\partial x\,\partial\phi}+F_c\frac{\partial^2 v_{c-f}}{\partial x\,\partial\phi}\right)\right]\right\}.\end{aligned} \tag{23}$$

These and equations (3), (7) and (8) can be substituted into the expression for the power transmission (equation (16)) through any cylinder cross-section at axial location x to produce

$$P_{xa}=\frac{r}{2}\int_0^{2\pi}\mathrm{Re}\left[F_cF_c^*A+F_cF_p^*B+F_pF_c^*C+F_pF_p^*D\right]\mathrm{d}\phi \tag{24}$$

where

$$\begin{aligned}A=&-\frac{K}{r^3}\left(\frac{\partial^2 w_{c-f}}{\partial x^2}+\nu\frac{\partial^2 w_{c-f}}{\partial\phi^2}-\frac{\partial u_{c-f}}{\partial x}-\nu\frac{\partial v_{c-f}}{\partial\phi}\right)\frac{\partial^2 w_{c-f}^*}{\partial x\,\partial t}\\ &+\frac{K}{r^3}\left[\frac{\partial^3 w_{c-f}}{\partial x^3}+\nu\frac{\partial^3 w_{c-f}}{\partial x\,\partial\phi^2}-\frac{\partial^2 u_{c-f}}{\partial x^2}-\nu\frac{\partial^2 v_{c-f}}{\partial x\,\partial\phi}\right.\\ &\left.+(1-\nu)\left(\frac{\partial^3 w_{c-f}}{\partial x\,\partial\phi^2}+\frac{1}{2}\frac{\partial^2 u_{c-f}}{\partial\phi^2}-\frac{1}{2}\frac{\partial^2 v_{c-f}}{\partial x\,\partial\phi}\right)\right]\frac{\partial w_{c-f}^*}{\partial t}\\ &+\left(\frac{D_e}{r}\frac{\partial u_{c-f}}{\partial x}+\nu\frac{D_e}{r}\frac{\partial v_{c-f}}{\partial\phi}+\nu\frac{D_e}{r}w_{c-f}-\frac{K}{r^3}\frac{\partial^2 w_{c-f}}{\partial x^2}\right)\frac{\partial u_{c-f}^*}{\partial t}\\ &+\left(\frac{D_e}{r}\frac{1-\nu}{2}\frac{\partial u_{c-f}}{\partial\phi}+\frac{D_e}{r}\frac{1-\nu}{2}\frac{\partial v_{c-f}}{\partial x}\right.\\ &\left.+\frac{K}{r^3}\frac{1-\nu}{2}\frac{\partial v_{c-f}}{\partial x}-\frac{K}{r^3}\frac{1-\nu}{2}\frac{\partial^2 w_{c-f}}{\partial x\,\partial\phi}\right)\frac{\partial v_{c-f}^*}{\partial t}.\end{aligned} \tag{25}$$

The expressions for B, C and D are very similar to above expression for A. For example, to obtain B, replace c by p in the conjugate part of each term; to obtain C, replace c by

p in the non-conjugate part of each term; and to obtain D, replace c by p in both the conjugate and non-conjugate part of each term.

The optimal control force corresponding to minimum power transmission is obtained by determining derivatives of equation (24) with respect to the real and imaginary components of the control force and setting the derivatives equal to zero. The result is

$$F_c^{opt} = \frac{\int_0^{2\pi} B^* \, \mathrm{d}\phi + \int_0^{2\pi} C \, \mathrm{d}\phi}{2 \int_0^{2\pi} \mathrm{Re}\,[A] \, \mathrm{d}\phi} F_p. \tag{26}$$

4.2. MINIMIZATION OF POWER TRANSMISSION WITH A LINE OF THREE INDEPENDENTLY DRIVEN POINT CONTROL FORCES

For this case, the cylindrical displacement w, u and v obtained from equations (3), (7) and (8) can be substituted into equations (A26) and (17)–(19). The results from these equations can then be substituted into equation (16), to give an expression for the total power transmission. The total power transmission can be written in matrix form as:

$$P_{xa} = \frac{r}{2} \int_0^{2\pi} \mathrm{Re}\,[\mathbf{F}^{\mathrm{H}}, \mathbf{AF}] \, \mathrm{d}\phi, \tag{27}$$

where

$$\mathbf{F} = [F_p, F_{c1}, F_{c2}, F_{c3}]^{\mathrm{T}} \tag{28}$$

and

$$\mathbf{A} = \begin{bmatrix} A(1,1) & A(1,2) & A(1,3) & A(1,4) \\ A(2,1) & A(2,2) & A(2,3) & A(2,4) \\ A(3,1) & A(3,2) & A(3,3) & A(3,4) \\ A(4,1) & A(4,2) & A(4,3) & A(4,4) \end{bmatrix}; \tag{29}$$

and superscript H is the complex conjugate and transpose of a matrix. The coefficients $A(i, j)$ ($i = 1, 4$, $j = 1, 4$) of matrix $\mathbf{A}$ result from the product of terms in equation (16), each of which contains contributions from the four different force elements of equation (28). The expressions for $A(i, j)$ ($i = 1, 4$, $j = 1, 4$) are very similar to the above expression for A in equation (25). There is only one change to the expression in each case. For example, to obtain $A(1, 1)$, replaced c by p in both the conjugate and non-conjugate parts of each term; to obtain $A(2, 1)$, replace p by $c1$ in the non-conjugate part of each term.

An optimal set of control forces corresponding to minimum power transmission is obtained by determining derivatives of equation (27) with respect to the real and imaginary components of each control force and setting the derivatives equal to zero. An optimum set of control forces corresponding to a minimum power transmission due to three

independent radial control forces is

$$\begin{bmatrix} F_{c1} \\ F_{c2} \\ F_{c3} \end{bmatrix} =$$

$$- \begin{bmatrix} \int_0^{2\pi} (A^*(2,2) + A(2,2))\,\mathrm{d}\phi & \int_0^{2\pi} (A^*(3,2) + A(2,3))\,\mathrm{d}\phi & \int_0^{2\pi} (A^*(4,2) + A(2,4))\,\mathrm{d}\phi \\ \int_0^{2\pi} (A^*(2,3) + A(3,2))\,\mathrm{d}\phi & \int_0^{2\pi} (A^*(3,3) + A(3,3))\,\mathrm{d}\phi & \int_0^{2\pi} (A^*(4,3) + A(3,4))\,\mathrm{d}\phi \\ \int_0^{2\pi} (A^*(2,4) + A(4,2))\,\mathrm{d}\phi & \int_0^{2\pi} (A^*(3,4) + A(4,3))\,\mathrm{d}\phi & \int_0^{2\pi} (A^*(4,4) + A(4,4))\,\mathrm{d}\phi \end{bmatrix}^{-1}$$

$$\times \left(\begin{bmatrix} \int_0^{2\pi} A^*(1,2)\,\mathrm{d}\phi \\ \int_0^{2\pi} A^*(1,3)\,\mathrm{d}\phi \\ \int_0^{2\pi} A^*(1,4)\,\mathrm{d}\phi \end{bmatrix} + \begin{bmatrix} \int_0^{2\pi} A(2,1)\,\mathrm{d}\phi \\ \int_0^{2\pi} A(3,1)\,\mathrm{d}\phi \\ \int_0^{2\pi} A(4,1)\,\mathrm{d}\phi \end{bmatrix} \right) F_p. \quad (30)$$

By comparing equations (26) with (30) and (24) with (27), it can be seen that the single force changes to a force vector when in-phase force control changes to independent force control. The expression for the power transmission given by equation (27) not only includes each force term, but also includes coupling force terms, which makes independent force control much more complex than in-phase force control to analyze.

The procedure can be used for any number of independently controlled forces. For six control sources, the corresponding (7×1) force matrix is:

$$\mathbf{F} = \begin{bmatrix} F_p \\ F_{c1} \\ F_{c2} \\ F_{c3} \\ F_{c4} \\ F_{c5} \\ F_{c6} \end{bmatrix}. \quad (31)$$

The analyses shown in sections 2 and 4 are for radial forces. Similar analyses can be applied to axial and circumferential forces, and also to corresponding acceleration and power transmission cost functions.

5. NUMERICAL RESULTS

The numerical results presented in this section have been calculated for a steel cylinder with Young's modulus $E = 207$ GPa, density $\rho = 7700$ kg/m^3 and Poisson ratio $v = 0{\cdot}3$. With the exception of section 5·5, the radius, thickness and excitation frequency are held constant at $r = 0{\cdot}25$ m, $h = 0{\cdot}003$ m and $f = 510$ Hz. One end of the cylinder is assumed to be terminated anechoically and the other is simply supported. By way of example, the configuration selected for the numerical analysis included three in-phase primary; i.e., excitation, forces and three control forces. This selection was based on experience with semi-infinite plates, where it was found that three independent control forces gave better power transmission reduction (when single or three in-phase primary forces are used) than either single or multiple in-phase control forces. In section 5.5, results are given for varying radii, thicknesses and excitation frequencies.

5.1. DEFINITION OF THE NEAR FIELD

The near field of a vibration source of free field is the region near the source in which the amplitude of reactive power fluctuation is not negligible. The boundary between near and far fields is defined for convenience to be the point at which the reactive power fluctuation is 20 dB less than the corresponding active power. At and below this level, the effects of reactive power fluctuation are considered to be relatively insignificant. The radius of the near field is then $x/\lambda_f = 0{\cdot}73$ m ($\lambda_f = 0{\cdot}9632$ m is the flexural wavelength calculated from equation (A24)). That is, points further than $0{\cdot}73\lambda_f$ from the source are considered to be in the far field of the source. It should be noted that the transition from near to far fields is gradual, and a fixed location is chosen here only for convenience.

The definition of the near field can be used to define the near field of the extensional and torsional waves, because the extensional and torsional wave displacement has similar far field terms as shown in Appendix A.

5.2. POWER TRANSMISSION REDUCTION

In this section it is assumed that an ideal feedforward controller is available. It is also assumed that it is possible to obtain a measure of the vibratory power transmission along the cylinder, to be used as the controller error input. An experimental study of active control of the vibratory power transmission is discussed in reference [14].

The three radial primary actuators are all located at the same distance from the simply supported end of the cylinder. They are arranged around the circumference of the cylinder in ϕ co-ordinate locations of $2\pi/3$, $(4\pi/3) \times 1{\cdot}05$ and 2π. For each primary actuator, there is a corresponding radial control actuator sharing an identical ϕ co-ordinate location. The second (primary and control) actuators have been moved slightly from a symmetric position on the circumference. This is because the matrix that must be inverted in equation (30) is ill-conditioned if symmetric forces are applied. The primary forces are at $x_p = 0{\cdot}025$ m and the control forces are at $x_c - x_p = 0{\cdot}05$ m. The error sensors are at $x_e - x_p = 0{\cdot}54$ m, at which point the error sensors are close to the far field of the primary forces. The measurement points are at $x_{meas} - x_p = 2{\cdot}07$ m. The effect of the locations of error sensors and control forces will be discussed below. The cost function is the power transmitted past the error sensors.

In Table 1 are listed the different wave type power transmission reductions for three independently driven radial control forces, with the power transmitted by either the combined or individual wave types used for the cost function. The relative amplitudes and phases of the three control forces are also shown in the table for each error sensor case. In the first row of Table 1, "three waves" refers to flexural, extensional and torsional. In the three rows below, the individual wave types are considered separately.

This table shows that a total power transmission reduction of 30 dB can be achieved when the power transmitted by all three wave types is used as the cost function. It is possible to achieve a flexural wave power transmission reduction of 40 dB when only flexural wave power is used as the cost function, an extensional wave power transmission reduction is 30 dB when only extensional wave power is used as the cost function and a torsional wave power transmission reduction of 18 dB when only torsional wave power is used as the cost function. It can be seen that the reduction of the total power transmission is the same as that of the extensional wave power.

Comparing the uncontrolled power transmission P_{un} due to different wave types, it is found that the major contribution to power transmission is from extensional waves. The power transmission contribution due to flexural waves is small while for torsional waves it is negligible. This is because the axial force N_x shown in equation (17) is relatively large so that extensional wave power transmission P_e is greater than flexural wave power transmission P_f, even though the amplitude of the displacement of the extensional waves is smaller than that of the flexural waves.

5.3. EFFECT OF ERROR SENSOR TYPE, LOCATION AND NUMBER

In the examples discussed so far, the cost function which has been minimized is the vibratory intensity integrated around the circumference of the cylinder at some axial location x_e. This quantity is referred to as power transmission. Individual intensity measurements are used to supply the error input to a feedforward controller. However, vibratory intensity is not easily measured in practice. Thus the purpose of section 5.3 is to examine the effectiveness of using acceleration, which is more easily measured in practice, as the cost function. A theoretical comparison will be made of the total power

TABLE 1

Power transmission reduction for three independently driven radial control forces, and for either a combined or an individual wave type power transmission cost function

Wave type	$\lvert F_c\rvert/\lvert F_p\rvert$	$\phi_c - \phi_p$ (rad)	P_{un} (W)	P_{co} (W)	P.T. reduction (dB)
Three waves combined	0·74	3·11	0·19E − 07	0·20E − 10	30
	0·55	3·13			
	0·66	3·12			
Flexural wave	0·75	3·13	0·50E − 09	0·57E − 13	40
	0·55	3·13			
	0·67	3·13			
Extensional wave	0·74	3·11	0·18E − 07	0·19 E − 10	30
	0·55	3·13			
	0·66	3·12			
Torsional wave	0·71	−3·10	0·71E − 10	0·10E − 11	18
	0·55	3·04			
	0·64	3·10			

TABLE 2

The effect of different wave type cost functions on total power transmission reduction

Wave types	Acc. control,* $\lvert F_c\rvert/\lvert F_p\rvert$	$\phi_c - \phi_p$ (rad)	Total P.T. reduction (dB)	P.T. control,* $\lvert F_c\rvert/\lvert F_p\rvert$	$\phi_c - \phi_p$ (rad)	Total P.T. reduction (dB)
Three waves combined				0·74	3·11	30
				0·55	3·13	
				0·66	3·12	
Flexural wave	0·75	3·10	30	0·75	3·13	31
	0·56	3·13		0·55	3·13	
	0·67	3·11		0·67	3·13	
Extensional wave	0·73	−3·12	29	0·74	3·11	30
	0·55	3·13		0·55	3·13	
	0·65	−3·13		0·66	3·12	
Torsional wave	0·56	3·06	14	0·71	−3·10	23
	0·72	3·00		0·55	3·04	
	0·68	3·06		0·64	3·10	

* "Acc. control" refers to acceleration cost function and "P.T. control" refers to power transmission cost function, corresponding to the wave type shown in the first column.

transmission reduction obtained while using seven alternative cost functions including different wave type acceleration and different wave type power transmission. The different wave types include the three individual wave types and, in the case of power transmission, three waves combined.

The primary and control radial actuator locations are the same as shown above in section 5.2. For acceleration control of individual wave types, the cost function to be minimized is the sum of the squares of the wave acceleration amplitudes integrated around the circumference of the cylinder. In Table 2 are shown the effect of cost function for either acceleration or power transmission, with different wave types either combined or individually. Data for the three waves combined acceleration cost function has not been obtained, partly because of the complexity of calculation and partly because of the complexity of measurement in practice. The results show that, except for torsional wave cases, a similar reduction in total power transmission is obtained when the cost function uses acceleration or power transmission for different wave types. Thus, either flexural or axial acceleration cost functions can be considered to be alternatives to the total power transmission cost function. In practice, flexural acceleration as the cost function is considered to be more easily measured. Therefore, the flexural acceleration cost function can be used as a suitable alternative to the total power transmission cost function. In the following analysis, both the flexural wave acceleration cost function and the total power transmission cost function are included.

In Table 3, four different axial locations are tried for the error sensor locations. The calculated power transmission reduction corresponding to each axial location of the error sensors using flexural acceleration as the cost function, is then compared with that found using total power transmission as the cost function. The total power transmission reduction is dependent on the error sensor locations for both cost functions. The reduction increases when the error sensor/control source axial separation $x_e - x_c$ increases. However, the reduction does not continue to increases significantly when $x_e - x_c > 0{\cdot}49$ m, at which point the error sensors are close to the far field of the primary forces. The reduction is

a constant when $x_e - x_c > 0{\cdot}69$ m at which point the error sensors are in the far field of the control forces. The reduced reduction in total power transmission when the error sensors are in the near field of the control forces, i.e., when $x_e - x_c < 0{\cdot}69$ m, is due to the fact that the near field reactive power fluctuations affect the ability of the error sensors properly to observe the power transmission. The results further show that the total reduction resulting from using the flexural acceleration cost function is approximately the same as that obtained by using total power transmission as the cost function. This applies for each of four error sensor locations.

In practice, it is not possible to integrate the vibratory intensity around the circumference of the cylinder, although it is possible to integrate the flexural acceleration by using a PVDF film sensor [15]. However, in some instances, the acceleration will be measured by a number of accelerometers at discrete points. It is of interest to examine the effect on the maximum achievable reduction in power transmission of deriving the cost functions by averaging over a fixed number of sensors rather than integrating around the full circumference of the cylinder.

In Table 4 are shown results that demonstrate the effect of changing within the range of 3 to 199 the number of error sensors (accelerometers for acceleration and accelerometer pairs for power transmission [14]), for locations at $x_e - x_c = 0{\cdot}49$ m. The error sensors are spaced in a line around the circumference of the cylinder. Two important results are obtained. The power transmission reduction is constant for error sensor numbers in the range of 9 to 199. Also, the power transmission reduction is equal both for the acceleration cost function and for the total power transmission cost function in the range of 9 to 199. From this table, it can be seen that only three flexural acceleration error sensors are necessary, because the results are similar to those obtained when using power transmission cost function with 199 error sensors. For three and seven error sensors, the reductions obtained by using power transmission as the cost function are not presented in this table. This is because the expression for power transmission given by equation (27) is inaccurate when less than nine power transmission error sensors are used. Use of less than three error sensors results in an under-determined system, which causes one of the three control forces

TABLE 3

The effect of error sensor type and location on total power transmission reduction

Location, $x_e - x_c$ (m)	Acc. control, $\lvert F_c\rvert/\lvert F_p\rvert$	$\phi_c - \phi_p$ (rad)	Total P.T. reduction (dB)	P.T. control, $\lvert F_c\rvert/\lvert F_p\rvert$	$\phi_c - \phi_p$ (rad)	Total P.T. reduction (dB)
0·29	0·71	3·11	25	0·71	−3·11	25
	0·54	3·12		0·54	3·13	
	0·64	3·12		0·64	−3.13	
0·49	0·75	3·10	30	0·74	3·11	30
	0·56	3·13		0·55	3·13	
	0·67	3·11		0·66	3·12	
0·69	0·77	3·12	31	0·76	3·11	31
	0·56	3·14		0·56	3·14	
	0·68	3·13		0·68	3·13	
0·89	0·77	−3·14	31	0·77	3·13	31
	0·55	−3·14		0·55	−3·13	
	0·68	−3·14		0·68	−3·13	

TABLE 4

The effect of number of error sensors in a ring at a single axial location on total power transmission reduction

No. of error sensors	Acc. control, $\lvert F_c\rvert/\lvert F_p\rvert$	$\phi_c - \phi_p$ (rad)	Total P.T. reduction (dB)	P.T. control, $\lvert F_c\rvert/\lvert F_p\rvert$	$\phi_c - \phi_p$ (rad)	Total P.T. reduction (dB)
3	0·76	3·10	29	0·74	3·10	
	0·55	3·13		0·56	3·11	
	0·67	3·11		0·65	3·10	
7	0·75	3·11	29	0·75	3·12	
	0·56	3·14		0·55	−3·13	
	0·67	3·11		0·66	3·10	
9	0·75	3·10	30	0·74	3·12	30
	0·56	3·13	30	0·55	3·11	
	0·67	3·11		0·66	3·12	
19	0·75	3·10	30	0·74	3·11	30
	0·56	3·13		0·55	3·13	
	0·67	3·11		0·66	3·12	
39	0·75	3·10	30	0·74	3·11	30
	0·56	3·13		0·55	3·12	
	0·67	3·11		0·66	3·12	
199	0·75	3·10	30	0·74	3·11	30
	0·56	3·13		0·55	3·12	
	0·67	3·11		0·66	3·12	

to be redundant, and this is not analyzable. As the computer program used for calculations is only applicable when there is an odd number of error sensors, the results for even numbers of error sensors are not presented in this table. Note that the error sensors should not be spaced evenly; otherwise, all of the error sensors might be located at vibrational nodes for some of the modes.

5.4. EFFECT OF CONTROL FORCE TYPE AND LOCATION

In the examples discussed so far, the primary and control force types are all radial forces. In the example in section 5.4, consideration is given to the following alternative primary and control force types: application of radial forces only; application of axial forces only or application of circumferential forces only. For each of these cases the primary and control forces are of the same type, and the cost function to be minimized is the sum of the squares of the flexural acceleration amplitudes at the error sensors. For each case, two different control force locations were analyzed, and the primary actuator and error sensor locations were the same as those used in the earlier analysis outlined in section 5.2. The results are shown in Table 5. It is concluded that the radial force is more effective than the axial force and the circumferential force. The results also show that the reduction of power transmission decreases when the separation distance between the primary and control actuators increases. A numerical analysis shows that these are true for a range of separation distance within $0 < x_c - x_p \leq 0{\cdot}2$ m. As in practice the minimum achievable separation will probably be $x_c - x_p \geq 0{\cdot}05$ m, Table 5 shows that a reduction of 30 dB is achievable for $x_c - x_p = 0{\cdot}05$ m when flexural wave acceleration control and radial forces are used.

Note that some of the results for circumferential force F_c/F_p are very large in Table 5, which shows that the circumferential force is not effective in the control of power transmission.

As mentioned above, the results in Table 5 refer only to the use of flexural acceleration as the cost function. Similar analyses for alternative cost functions, using either flexural, extensional or total power transmission as the cost function, result in similar conclusions to those presented above. An example is shown in Table 2.

5.5. EFFECT OF THICKNESS, RADIUS AND FREQUENCY

It is known that measurement of power transmission is easier for flexural waves than for extensional waves. In section 5.2, it was shown that for the cases considered, extensional waves produced the major contribution to power transmission. The purpose of section 5.5 is to examine the effect of cylinder thickness, radius and excitation frequency on the relative importance of flexural waves to the total power.

In Table 6 is shown the uncontrolled power transmission as a function of the thickness h. The locations of the primary actuators and the error sensors are the same as shown in Table 4 and the cost function is flexural acceleration. Radial forces only are used as the primary forces. The results show that generally the ratio P_f/P_s, of flexural wave power transmission P_f to the total power transmission P_s, increases as h increases. In Table 7 is presented the uncontrolled power transmission as a function of the radius r, which shows a trend of increasing ratio P_f/P_s as r increases. In Table 8 is presented the uncontrolled

TABLE 5

The effect of control force type and location on total power transmission reduction for flexural acceleration as the cost function

Control force type	Location, $x_c - x_p$ (m)	Acc. control, $\lvert F_c\rvert/\lvert F_p\rvert$	$\phi_c - \phi_p$ (rad)	Total P.T. reduction (dB)
Radial	0·05	0·75	3·10	30
		0·56	3·13	
		0·67	3·11	
	0·20	2·87	0·72	27
		3·82	1·82	
		4·41	1·21	
Axial	0·05	0·11	0.81E − 2	15
		0·34E − 2	0·29E + 1	
		0·19E − 1	0·25E − 1	
	0·20	0·28E − 1	0·49E − 1	13
		0·14E − 1	0·19E − 1	
		0·48E − 2	0·64E − 1	
Circumferential	0·05	0·46	3·12	27
		0·46	3·12	
		0·56E + 13	−0·53	
	0·2	0·92	0·20E + 1	0
		0·79	0·19E + 1	
		0·49E + 15	0·31E + 1	

TABLE 6

The effect of cylinder thickness on the ratio of flexural to total power transmission

Thickness, h (m)	Radius, r (m)	Frequency, f (Hz)	Flexural P.T., P_f (W)	Total P.T., P_s (W)	P_f/P_s
0·001	0·5	510	0·2192E − 9	0·3773E − 6	0·00058097
0·008	0·5	510	0·5646E − 9	0·1821E − 7	0·03100494
0·010	0·5	510	0·5880E − 9	0·1351E − 7	0·04352331
0·040	0·5	510	0·3263E − 9	0·2643E − 8	0·12345819
0·050	1·0	510	0·7737E − 8	0·9059E − 8	0·85406777
0·060	1·0	510	0·6010E − 8	0·6949E − 8	0·86487264

TABLE 7

The effect of cylinder radius on the ratio of flexural to total power transmission

Thickness, h (m)	Radius, r (m)	Frequency, f (Hz)	Flexural P.T., P_f (W)	Total P.T., P_s (W)	P_f/P_s
0·003	0·1	510	0·8529E − 14	0·4070E − 11	0·00209351
0·003	0·3	510	0·1710E − 09	0·2772E − 07	0·00616883
0·003	0·5	510	0·1213E − 08	0·7764E − 07	0·01562339

TABLE 8

The effect of excitation frequency on the ratio of flexural to total power transmission

Thickness, h (m)	Radius, r (m)	Frequency, f (Hz)	Flexural P.T., P_f (W)	Total P.T., P_s (W)	P_f/P_s
0·003	0·5	110	0·4168E − 10	0·3856E − 7	0·00108091
0·003	0·5	210	0·9335E − 10	0·5924E − 7	0·00157579
0·003	0·5	430	0·2807E − 09	0·7732E − 7	0·00363036
0·003	0·5	510	0·4032E − 09	0·7764E − 7	0·00519319
0·003	0·5	610	0·6414E − 09	0·7525E − 7	0·00852358

power transmission as a function of the excitation frequency f and shows a trend of increasing ratio P_f/P_s as f increases.

Comparing Tables 6, 7 and 8, it can be seen that cylinder thickness has a more significant effect on the ratio P_f/P_s than radius or excitation frequency. However, the assumption in the analysis is that $r/h > 16$, so there is a limit as to how much h can be increased without increasing r. It is concluded that a very large diameter and very thick cylinder is necessary to obtain the flexural waves as the dominant waves in producing power transmission under the assumption of $r/h > 16$. The extensional waves remain the major factor in producing power transmission for most cylinders of a practical size. It is also concluded that, in most cases, the extensional wave power transmission gives a good approximation of the total power transmission. This conclusion provides an opportunity for simplification of power transmission measurement methods in experimental work involving error sensors either in or close to the far field of the control sources as is discussed in reference [14].

6. CONCLUSIONS

Harmonic power transmission in a semi-infinite cylinder can be reduced significantly by using an array of independently driven control forces around the circumference of the cylinder. For three or more radial control forces, it is theoretically possible to achieve a 30 dB reduction in power transmission for both acceleration and power transmission cost functions, under certain conditions. To achieve this reduction, it is necessary that the error sensors are either in or close to the flexural wave far field of the primary and control forces. It is also necessary that the control sources should be very close to primary sources and that the modelling conditions for the point forces can be achieved in practice. For the test cylinder, only three flexural acceleration error sensors are necessary if the error sensors are in the far field of the primary and control forces. It is concluded that, in general, a radial control force is more effective than an axial force or a circumferential force in controlling total power transmission. It is also suggested that use of either the flexural or the axial acceleration cost function can be an alternative to the total power transmission cost function.

It is interesting to note that one type of cost function (flexural or axial acceleration) can be effective on its own. This is because the flexural, extensional and torsional waves in cylinders are strongly coupled.

The study has also indicated that, in most cases, the extensional wave power transmission gives a good approximation of the total power transmission. This finding provides an opportunity for simplification of total power transmission measurement methods in experimental work.

REFERENCES

1. X. Pan and C. H. Hansen 1993 *Journal of Sound and Vibration* **165**, 497–510. Effect of error sensor location and type on the active control of beam vibration.
2. X. Pan and C. H. Hansen 1993 *Journal of Sound and Vibration* **168**, 429–448. Effect of end conditions on the active control of beam vibration.
3. X. Pan and C. H. Hansen 1995 *Journal of Sound and Vibration* **184**, 585–610. Active control of vibratory power transmission along a semi-infinite plate.
4. X. Pan, C. H. Hansen and S. D. Synder 1995 *International Journal of Active Control* **1**(2), 145–166. Power transmission characteristics in an actively controlled semi-infinite plate.
5. W. Flügge 1973 *Stresses in Shells*. Berlin: Springer-Verlag. See pages 204–259.
6. A. W. Leissa 1973 *Vibration of Shells*, *NASA SP*-288, 1–184.
7. K. Forsberg 1964 *American Institute of Aeronautics and Astronautics Journal* **2**(12), 2150–2157. Influence of boundary conditions on the modal characteristics of thin cylindrical shells.
8. K. Forsberg 1966 *NASA CR*-613. A review of analytical methods used to determine the modal characteristics of cylindrical shells.
9. C. R. Fuller and J. D. Jones 1987 *Journal of Sound and Vibration* **112**, 389–395. Experiments on reduction of propeller induced interior noise by active control of cylinder vibration.
10. J. D. Jones and C. R. Fuller 1989 *American Institute of Aeronautics and Astronautics Journal* **27**(7), 845–852. Active control of sound fields in elastic cylinders by multicontrol forces.
11. S. J. Elliott, P. A. Nelson, I. M. Stothers and C. C. Boucher 1989 *Journal of Sound and Vibration* **128**, 355–357. Preliminary results of in-flight experiments on the active control of propeller-induced cabin noise.
12. C. R. Fuller and B. J. Brevart 1995 *Active*, 2–13. Active control of coupled wave propagation and associated power in fluid-filled elastic long pipes.
13. R. J. Pinnington and A. R. Briscoe 1994 *Journal of Sound and Vibration* **173**, 503–516. Externally applied sensor for axisymmetric waves in a fluid filled pipe.
14. X. Pan and C. H. Hansen 1996 *The* 131*st Meeting of the Acoustical Society of America*, *Indianapolis*, *U.S.A*. An experimental study of active control of vibration transmission in a cylindrical shell.

15. G. P. Gibbs and C. R. Fuller 1990 *AIAM SDM Conference*, *Long Beach*, *California*, *U.S.A.*, 2331–2339. Experiments on active control of vibrational power flow using piezoceramic actuators and sensors.
16. X. Pan and C. H. Hansen 1994 *Journal of Intelligent Material Systems and Structures* **5** (3), 363–370. Piezoelectric crystal vs point force excitation of beams and plates.
17. C. R. Fuller 1981 *Journal of Sound and Vibration* **75**, 207–228. The effects of wall discontinuities on the propagation of flexural waves in cylindrical shells.
18. E. Skudrzyk 1965 *Simple and Complex Vibratory Systems*. University Park, Pennsylvania: The Pennsylvania State University Press. See pages 3–9.
19. B. J. Brevart and C. R. Fuller 1993 *Journal of Sound and Vibration* **167**, 149–163. Effect of an internal flow on the distribution of vibrational energy in an infinite fluid-filled thin cylindrical elastic shell.

APPENDIX A: THE RESPONSE OF A SEMI-INFINITE CYLINDER TO A LINE OF POINT FORCES DRIVEN IN PHASE

The extension of the classical equations of motion for a cylinder given by Flügge [5], with cylinder inertia included, is

$$u'' + \frac{1-\nu}{2}u^{\cdot\cdot} + \frac{1+\nu}{2}v'^{\cdot} + \nu w' + \xi\left[\frac{1-\nu}{2}u^{\cdot\cdot} - w''' + \frac{1-\nu}{2}w'^{\cdot\cdot}\right] - \gamma^2\frac{\partial^2 u}{\partial t^2} = -\gamma^2\frac{F_x}{\rho h}, \quad \text{(A1)}$$

$$\frac{1+\nu}{2}u'^{\cdot} + v^{\cdot\cdot} + \frac{1-\nu}{2}v'' + w^{\cdot} + \xi\left[\frac{3(1-\nu)}{2}v'' - \frac{3-\nu}{2}w''^{\cdot}\right] - \gamma^2\frac{\partial^2 v}{\partial t^2} = -\gamma^2\frac{F_\phi}{\rho h} \quad \text{(A2)}$$

and

$$\nu u' + v^{\cdot} + w + \xi\left[\frac{1-\nu}{2}u'^{\cdot\cdot} - u''' - \frac{3-\nu}{2}v''^{\cdot} + w^{IV} + 2w''^{\cdot\cdot} + w^{\cdot\cdot\cdot\cdot} + 2w^{\cdot\cdot} + w\right] + \gamma^2\frac{\partial^2 w}{\partial t^2} = \gamma^2\frac{F_r}{\rho h}, \quad \text{(A3)}$$

where the quantities $u = (x, \phi, t)$, $v = v(x, \phi, t)$ and $w = w(x, \phi, t)$ are the displacements in the axial, circumferential and radial directions respectively, and F_x, F_ϕ and F_r are the applied forces per unit surface area in each direction. The derivatives with respect to the dimensionless co-ordinates x/r and ϕ will be indicated by primes and dots:

$$r\frac{\partial(\,)}{\partial x} = (\,)', \qquad \frac{\partial(\,)}{\partial\phi} = (\,)^{\cdot}.$$

The geometry of the cylinder and co-ordinates are shown in Figure 1 and the sign conventions are shown in Figure 2. The cylinder is simply supported at $x = 0$ and is infinite at the other end.

As the cylinder is closed, the following harmonic series solutions in ϕ can be assumed for cylinder vibrational displacement in the axial, circumferential and radial directions (developed by Flügge [5], also later used by Brevart and Fuller [19]):

$$u(x, \phi, t) = \sum_{n=1}^{\infty} u_n(x) \cos n\phi \; e^{j\omega t}, \tag{A4}$$

$$v(x, \phi, t) = \sum_{n=1}^{\infty} v_n(x) \sin n\phi \; e^{j\omega t} \tag{A5}$$

and

$$w(x, \phi, t) = \sum_{n=1}^{\infty} w_n(x) \cos n\phi \; e^{j\omega t}, \tag{A6}$$

where n is the circumferential mode number. Each of the eigenfunctions $u_n(x)$, $v_n(x)$ and $w_n(x)$ can be expressed in terms of the modal wavenumbers k_{sn} as follows [7]:

$$u_n(x) = \sum_{s=1}^{8} \alpha_{sn} A_{sn} \, e^{k_{sn} x/r}, \qquad v_n(x) = \sum_{s=1}^{8} \beta_{sn} A_{sn} \, e^{k_{sn} x/r} \tag{A7, A8}$$

and

$$w_n(x) = \sum_{s=1}^{8} A_{sn} \, e^{k_{sn} x/r}, \tag{A9}$$

where A_{sn}, α_{sn} and β_{sn} are arbitrary constants. Equations (A7), (A8) and (A9) show that the eigenfunctions depend on the circumferential mode only. This is because in the semi-infinite cylinder there is no axial mode and the circumferential modes are the only modes available. It will be explained below that, for a single circumferential mode, there are eight eigenvalues (i.e., wavenumbers k_{sn}, $s = 1, 2, \ldots, 8$).

A.1. DETERMINING THE WAVENUMBERS AND CONSTANTS α AND β

For each mode, the homogeneous form of equations (A1), (A2) and (A3) must be satisfied. To find the modal wavenumbers, we take the general term of equations (A4), (A5) and (A6), put $u = u_n(x) \cos n\phi$, $v = v_n(x) \sin n\phi$, $w = w_n(x) \cos n\phi$, and introduce this into the homogeneous form of equations (A1), (A2) and (A3). All the terms in each equation have a common factor $\sin n\phi$ or $\cos n\phi$, which cancels to give

$$u_n'' - \frac{1-\nu}{2} n^2 u_n + \frac{1+\nu}{2} n v_n' + \nu w_n' - \xi\left[\frac{1-\nu}{2} n^2 u_n + w_n''' + \frac{1-\nu}{2} n^2 w_n'\right] + \omega\gamma^2 u_n = 0, \tag{A10}$$

$$-\frac{1+\nu}{2} n u_n' - n^2 v_n + \frac{1-\nu}{2} v_n'' - n w_n + \xi\left[\frac{3(1-\nu)}{2} v_n'' + \frac{3-\nu}{2} n w_n''\right] + \omega^2\gamma^2 v_n = 0 \tag{A11}$$

and

$$\nu u_n' + n v_n + w_n + \xi$$

$$\left[-\frac{1-\nu}{2} n^2 u_n' - u_n''' - \frac{3-\nu}{2} n v_n'' + w_n^{IV} - 2n^2 w_n'' + n^4 w_n - 2n^2 w_n + w_n\right] - \omega\gamma^2 w_n = 0. \tag{A12}$$

Equations (A10), (A11) and (A12) have constant coefficients and may be solved by exponential functions:

$$u_n = A_n \, \mathrm{e}^{k_{sn}x/r}, \qquad v_n = B_n \, \mathrm{e}^{k_{sn}x/r} \qquad \text{and} \qquad w_n = C_n \, \mathrm{e}^{k_{sn}x/r}.$$

After introducing this into equations (A10), (A11) and (A12), we may drop the exponential factor and then have three ordinary linear equations for the constants A_n, B_n and C_n.

$$\left[k_{sn}^2 - \frac{1-\nu}{2} n^2(1+\xi) + \omega^2\gamma^2\right]A_n + \frac{1+\nu}{2} k_{sn} n B_n + \left[\nu k_{sn} - \xi\left(k_{sn}^3 + \frac{1-\nu}{2} k_{sn} n^2\right)\right]C_n = 0, \tag{A13}$$

$$\frac{1+\nu}{2} k_{sn} n A_n + \left[-\frac{1-\nu}{2} k_{sn}^2 + n^2 - \frac{3(1-\nu)}{2} \xi k_{sn}^2 + \omega^2\gamma^2\right]B_n + \left[n - \frac{3-\nu}{2} \xi k_{sn}^2 n\right]C_n = 0 \tag{A14}$$

and

$$\left[\nu k_{sn} - \xi\left(k_{sn}^3 + \frac{1-\nu}{2} k_{sn} n^2\right)\right]A_n + \left[n - \frac{3-\nu}{2} \xi k_{sn}^2 n\right]B_n + [1 + \xi(k_{sn}^4 - 2k_{sn}^2 n^2 + n^4 - 2n^2 + 1) - \omega^2\gamma^2]C_n = 0. \tag{A15}$$

Since these equations are homogeneous, they can have a solution A_n, B_n and C_n different from zero only if the determinant formed from their nine coefficients vanishes. This condition can be used to determine k_{sn}. In general, the solution will usually have the form [7]

$$k_{1n} = -a, \qquad k_{2n} = -\mathrm{j}b, \qquad k_{3n} = -(c + \mathrm{j}d), \qquad k_{4n} = -(c - \mathrm{j}d),$$

$$k_{5n} = +a, \qquad k_{6n} = +\mathrm{j}b, \qquad k_{7n} = +(c + \mathrm{j}d), \qquad k_{8n} = +(c - \mathrm{j}d)$$

where a, b, c and d are real quantities. The above wavenumber equations show that, for a single circumferential mode, there are eight wavenumbers. This is because the wavenumbers consist of near and far field terms in two opposite directions (k_{1n}, k_{2n}, k_{5n} and k_{6n}) and the terms resulting from torsional motion (k_{3n}, k_{4n}, k_{7n} and k_{8n}). These wavenumbers are different to the form of the solutions given by Flügge [5], because the inertia terms have been included here.

The constant α_n and β_n ($n = 1, \ldots, \infty$) can now be found from any two of equations (A13), (A14) and (A15). Using the definition of $A_n = \alpha_n C_n$ and $B_n = \beta_n C_n$ ($n = 1, \ldots, \infty$), the complex numbers α_n and β_n can be determined by assuming $C_n = 1$ ($n = 1, \ldots, \infty$) in equations (A13), (A14) and (A15).

On each side of an applied force at $x = x_0$, each eigenfunction is a different linear combination of the terms $\mathrm{e}^{k_{sn}x/r}$. For $x < x_0$,

$$u_{1n}(x) = \sum_{s=1}^{8} \alpha_{sn} A_{1sn} \, \mathrm{e}^{k_{sr}x/r}, \qquad v_{1n}(x) = \sum_{s=1}^{8} \beta_{sn} A_{1sn} \, \mathrm{e}^{k_{sn}x/r}, \tag{A16, A17}$$

and

$$w_{1n}(x) = \sum_{s=1}^{8} A_{1sn}\, \mathrm{e}^{k_{sn}x/r}. \tag{A18}$$

For $x > x_0$,

$$u_{2n}(x) = \sum_{s=1}^{4} \alpha_{sn} A_{2sn}\, \mathrm{e}^{k_{sn}x/r}, \qquad v_{2n}(x) = \sum_{s=1}^{4} \beta_{sn} A_{2sn}\, \mathrm{e}^{k_{sn}x/r} \tag{A19, A20}$$

and

$$w_{2n}(x) = \sum_{s=1}^{4} A_{2sn}\, \mathrm{e}^{k_{sn}x/r}. \tag{A21}$$

Note that in equations (A19), (A20) and (A21), A_{25n} to A_{28n} have been omitted because, for a semi-infinite cylinder, there is no boundary to produce reflected waves with a negative horizontal velocity component.

A2. DETERMINING THE FLEXURAL WAVELENGTH

The flexural wavelength can be obtained from the homogeneous form of equation (A3). The flexural wavelength can be obtained by dividing both sides of the homogeneous form of equation (A.3) by ξ, and using the definitions of ξ and γ^2 (see list of symbols) to obtain

$$\frac{1}{\xi}(vu' + v^{\cdot} + w) + \left[\frac{1-v}{2}u'^{\cdot\cdot} - u''' - \frac{3-v}{2}v''^{\cdot} + w^{IV} + 2w''^{\cdot\cdot} + w^{\cdot\cdot\cdot\cdot} + 2w^{\cdot\cdot} + w\right] - \frac{\omega^4}{\omega^2 Eh^2/[12\rho(1-v^2)r^4]}w = 0. \tag{A22}$$

Following a similar procedure to that used for the calculation of the flexural wavelength in a flat plate, the coefficient of the last term in equation (A22) may be expressed as

$$\frac{\omega^4}{\omega^2 Eh^2/[12\rho(1-v^2)r^4]} = k_f^4. \tag{A23}$$

Equation (A23) can also be written as

$$k_f = \omega/c_f = 2\pi/\lambda_f \tag{A24}$$

and

$$c_f = \left(\sqrt{\frac{\omega^2 Eh^2}{12\rho(1-v^2)r^4}}\right)^{1/4}, \tag{A25}$$

which is the expression for the frequency dependent flexural wave speed in the cylinder. Note that the flexural wave speed is the ratio of the flexural wave speed in a flat plate of thickness equal to that of the cylinder, to the radius of the cylinder.

A.3. SIMPLY SUPPORTED END CONDITIONS

The four boundary conditions corresponding to a simple support are $u = 0$, $v = 0$, $w = 0$ and $M_x = 0$ given by Leissa [6], where M_x was given by Flügge [5]:

$$M_x = (K/r^2)(w'' + vw^{\cdot\cdot} - u' - vv^{\cdot}). \tag{A26}$$

In terms of the displacement unknowns, these boundary conditions for a simply supported end at $x = 0$ are

$$\sum_{s=1}^{8} \alpha_{sn} A_{1sn} = 0, \qquad \sum_{s=1}^{8} \beta_{sn} A_{1sn} = 0, \qquad \sum_{s=1}^{8} A_{1sn} = 0 \tag{A27–A29}$$

and

$$\sum_{s=1}^{8} (k_{sn}^2 - vn^2 - \alpha_{sn} k_{sn} - vn\beta_{sn}) A_{1sn} = 0. \tag{A30}$$

A.4. EQUILIBRIUM CONDITIONS AT THE POINT OF AN APPLIED FORCE

Requiring that the displacement and its gradient in each direction be continuous at any point in the cylinder wall, the first six equilibrium conditions at $x = x_0$ which must be satisfied are

$$u_{1n} = u_{2n}, \quad u'_{1n} = u'_{2n}, \quad v_{1n} = v_{2n}, \quad v'_{1n} = v'_{2n}, \quad w_{1n} = w_{2n}, \quad w'_{1n} = w'_{2n}. \tag{A31–A36}$$

The form of the excitation F will affect the higher order equilibrum conditions at $x = x_0$.

The displacement response of the cylinder to an array of m equally spaced radial point forces around a circumference of the cylinder at positions $((x_0, \phi_i), i = 1, \ldots, m)$ is considered. The radial force F_r in equation (A3) is assumed to be driven in-phase and with the same complex amplitude F_0 so that

$$F_r = F_0 \sum_{i=1}^{m} \delta(x - x_0)\delta(\phi - \phi_i)\, e^{j\omega t}. \tag{A37}$$

Replacing u, v and w by equations (A4)–(A6), dividing by $e^{j\omega t}$, multiplying by $\cos n\phi$ and taking integral from $-\pi$ to π with respect to ϕ, equation (A3) can be written as

$$vu'_n(x) + mv_n(x) + w_n(x) + \xi\left[-\frac{1-v}{2} n^2 u'_n(x) - u'''_n(x) - \frac{3-v}{2} m v''_n(x) \right.$$

$$\left. + w_n^{IV}(x) - 2m^2 w''_n(x) + m^4 w_n(x) - 2m^2 w_n(x) + w_n(x) \right] - \gamma^2 \omega^2 w_n(x)$$

$$= \frac{\gamma^2 F_0 \delta(x - x_0)}{\pi \rho h} \sum_{i=1}^{m} \cos \phi_i. \tag{A38}$$

Then taking the integral from $x_0 - \delta$ to $x_0 + \delta$ with respect to x in this equation, using the conditions

$$\int_{x_0-\delta}^{x_0+\delta} w_n(x)\,\mathrm{d}x \to 0, \qquad \int_{x_0-\delta}^{x_0+\delta} w_n'(x)\,\mathrm{d}x \to 0 \tag{A39, A40}$$

(similarly for $u_n(x)$, $v_n(x)$, $u_n'(x)$ and $v_n'(x)$) and

$$\int_{x_0-\delta}^{x_0+\delta} w_n''(x)\,\mathrm{d}x \to 0 \tag{A41}$$

as $\delta \to 0$, we obtain

$$-\int_{x_0-\delta}^{x_0+\delta} u_n'''(x)\,\mathrm{d}x + \int_{x_0-\delta}^{x_0+\delta} w_n^{IV}(x)\,\mathrm{d}x = \frac{F_0\gamma^2}{\pi\rho h\xi}\sum_{i=1}^{m}\cos\phi_i \int_{x_0-\delta}^{x_0+\delta}\delta(x-x_0)\,\mathrm{d}x \tag{A42}$$

or

$$u_{1n}''(x_0) - u_{2n}''(x_0) + w_{2n}'''(x_0) - w_{1n}'''(x_0) = \frac{F_0\gamma^2}{\pi\rho h\xi}\sum_{i=1}^{m}\cos\phi_i. \tag{A43}$$

Finally, taking the integral from $x_0 - \delta$ to $x_0 + \delta$ with respect to x in equation (A43), we obtain

$$w_{1n}''(x_0) = w_{2n}''(x_0). \tag{A44}$$

A.5. DETERMINATION OF THE EIGENVECTOR

For a semi-infinite cylinder with the end at $x = 0$ modelled as simply supported, equations (A27)–(A36), (A44) and (A43) can be written as a 12×12 matrix equation. We use the definition of $M_i = k_{in}^2 - vn^2 - \alpha_{in}k_{in} - v_{mn}\beta_{in}$ $(i = 1, \ldots, 8)$ in equation (A30). Substituting equations (A7), (A8) and (A9) into equation (A43), in terms of the eigenvector unknowns, the coefficients in equation (A43) can be written as $F_i = \alpha_{in}k_{in}^2\,\mathrm{e}^{k_{in}x_0} - k_{in}^3\,\mathrm{e}^{k_{in}x_0}$ $(i = 1, \ldots, 8)$ and $F_i = k_{(i-8)n}^3\,\mathrm{e}^{k_{(i-8)n}x_0} - \alpha_{(i-8)n}\,k_{(i-8)n}^2\,\mathrm{e}^{k_{(i-8)n}x_0}$ $(i = 9, \ldots, 12)$. The 12×12 matrix equation can be written as:

$$
\begin{bmatrix}
\alpha_{1n} & \alpha_{2n} & \alpha_{3n} & \alpha_{4n} & \alpha_{5n} & \alpha_{6n} & \alpha_{7n} & \alpha_{8n} & 0 & 0 & 0 & 0 \\
\beta_{1n} & \beta_{2n} & \beta_{3n} & \beta_{4n} & \beta_{5n} & \beta_{6n} & \beta_{7n} & \beta_{8n} & 0 & 0 & 0 & 0 \\
1 & 1 & 1 & 1 & 1 & 1 & 1 & 1 & 0 & 0 & 0 & 0 \\
M_1 & M_2 & M_3 & M_4 & M_5 & M_6 & M_7 & M_8 & 0 & 0 & 0 & 0 \\
\alpha_{1n}e^{k_{1n}x_0} & \alpha_{2n}e^{k_{2n}x_0} & \alpha_{3n}e^{k_{3n}x_0} & \alpha_{4n}e^{k_{4n}x_0} & \alpha_{5n}e^{k_{5n}x_0} & \alpha_{6n}e^{k_{6n}x_0} & \alpha_{7n}e^{k_{7n}x_0} & \alpha_{8n}e^{k_{8n}x_0} & \alpha_{1n}e^{k_{1n}x_0} & \alpha_{2n}e^{k_{2n}x_0} & \alpha_{3n}k_{3n}e^{k_{3n}x_0} & \alpha_{4n}k_{4n}e^{k_{4n}x_0} \\
\alpha_{1n}k_{1n}e^{k_{1n}x_0} & \alpha_{2n}k_{2n}e^{k_{2n}x_0} & \alpha_{3n}k_{3n}e^{k_{3n}x_0} & \alpha_{4n}k_{4n}e^{k_{4n}x_0} & \alpha_{5n}k_{5n}e^{k_{5n}x_0} & \alpha_{6n}k_{6n}e^{k_{6n}x_0} & \alpha_{7n}k_{7n}e^{k_{7n}x_0} & \alpha_{8n}k_{8n}e^{k_{8n}x_0} & -\alpha_{1n}k_{1n}e^{k_{1n}x_0} & -\alpha_{2n}k_{2n}e^{k_{2n}x_0} & -\alpha_{3n}k_{3n}e^{k_{3n}x_0} & -\alpha_{4n}k_{4n}e^{k_{4n}x_0} \\
\beta_{1n}e^{k_{1n}x_0} & \beta_{2n}e^{k_{2n}x_0} & \beta_{3n}e^{k_{3n}x_0} & \beta_{4n}e^{k_{4n}x_0} & \beta_{5n}e^{k_{5n}x_0} & \beta_{6n}e^{k_{6n}x_0} & \beta_{7n}e^{k_{7n}x_0} & \beta_{8n}e^{k_{8n}x_0} & -\beta_{1n}e^{k_{1n}x_0} & -\beta_{2n}e^{k_{2n}x_0} & -\beta_{3n}e^{k_{3n}x_0} & -\beta_{4n}e^{k_{4n}x_0} \\
\beta_{1n}k_{1n}e^{k_{1n}x_0} & \beta_{2n}k_{2n}e^{k_{2n}x_0} & \beta_{3n}k_{3n}e^{k_{3n}x_0} & \beta_{4n}k_{4n}e^{k_{4n}x_0} & \beta_{5n}k_{5n}e^{k_{5n}x_0} & \beta_{6n}k_{6n}e^{k_{6n}x_0} & \beta_{7n}k_{7n}e^{k_{7n}x_0} & \beta_{8n}k_{8n}e^{k_{8n}x_0} & -\beta_{1n}k_{1n}e^{k_{1n}x_0} & -\beta_{2n}k_{2n}e^{k_{2n}x_0} & -\beta_{3n}k_{3n}e^{k_{3n}x_0} & -\beta_{4n}k_{4n}e^{k_{4n}x_0} \\
e^{k_{1n}x_0} & e^{k_{2n}x_0} & e^{k_{3n}x_0} & e^{k_{4n}x_0} & e^{k_{5n}x_0} & e^{k_{6n}x_0} & e^{k_{7n}x_0} & e^{k_{8n}x_0} & -e^{k_{1n}x_0} & -e^{k_{2n}x_0} & -e^{k_{3n}x_0} & -e^{k_{4n}x_0} \\
k_{1n}e^{k_{1n}x_0} & k_{2n}e^{k_{2n}x_0} & k_{3n}e^{k_{3n}x_0} & k_{4n}e^{k_{4n}x_0} & k_{5n}e^{k_{5n}x_0} & k_{6n}e^{k_{6n}x_0} & k_{7n}e^{k_{7n}x_0} & k_{8n}e^{k_{8n}x_0} & -k_{1n}e^{k_{1n}x_0} & -k_{2n}e^{k_{2n}x_0} & -k_{3n}e^{k_{3n}x_0} & -k_{4n}e^{k_{4n}x_0} \\
k_{1n}^2e^{k_{1n}x_0} & k_{2n}^2e^{k_{2n}x_0} & k_{3n}^2e^{k_{3n}x_0} & k_{4n}^2e^{k_{4n}x_0} & k_{5n}^2e^{k_{5n}x_0} & k_{6n}^2e^{k_{6n}x_0} & k_{7n}^2e^{k_{7n}x_0} & k_{8n}^2e^{k_{8n}x_0} & -k_{1n}^2e^{k_{1n}x_0} & -k_{2n}^2e^{k_{2n}x_0} & -k_{3n}^2e^{k_{3n}x_0} & k_{4n}^2e^{k_{4n}x_0} \\
F_1 & F_2 & F_3 & F_4 & F_5 & F_6 & F_7 & F_8 & F_9 & F_{10} & F_{11} & F_{12}
\end{bmatrix}
\times
\begin{bmatrix}
A_{11n} \\ A_{12n} \\ A_{13n} \\ A_{14n} \\ A_{15n} \\ A_{16n} \\ A_{17n} \\ A_{18n} \\ A_{21n} \\ A_{22n} \\ A_{23n} \\ A_{24n}
\end{bmatrix}
=
\begin{bmatrix}
0 \\ 0 \\ 0 \\ 0 \\ 0 \\ 0 \\ 0 \\ 0 \\ 0 \\ 0 \\ 0 \\ \dfrac{F_0\hat{y}_i^2}{\pi\rho h_\zeta^2}\sum_{i=1}^{m}\cos\phi_i
\end{bmatrix}, \tag{A45}
$$

which can be written as $[\alpha][\mathbf{X}] = [\mathbf{F}]$. For each value of n, the solution $[\mathbf{X}]$ of the 12×12 system of equations is an eigenvector which describes modal shapes and amplitudes corresponding to the three different wave types (flexural, axial and circumferential).

The cylinder displacement at any location (x, ϕ) due to a line of in-phase radial point forces is

$$u = F_0\, u_{0-f}, \qquad v = F_0\, v_{0-f}, \qquad w = F_0\, w_{0-f}, \tag{A46–A48}$$

where u_{0-f}, v_{0-f} and ω_{0-f} are the displacements to unit radial force excitation which are obtained by solving equation (A45) and substituting the results for A_{1sn} ($s = 1, \ldots, 8$) and A_{2sn} ($s = 1, 2, 3, 4$) into equations (A16)–(A21) and (A4)–(A6). Similarly, the displacement responses due to unit axial force excitation or circumferential force excitation can be obtained by using equation (A1) or (A2) correspondingly.

APPENDIX B: LIST OF SYMBOLS

c_f flexural wave speed
D_e $= Eh/(1 - \nu^2)$, extensional rigidity
E Young's modulus
f excitation frequency
F point force
F_c control point force
F_0 complex point force amplitude
F_p primary point force
F_r radial force per unit surface area
F_x axial force per unit surface area
F_ϕ circumferential force per unit surface area
h cylinder shell thickness
j $= \sqrt{-1}$, complex unit
K $= Eh^3/[12(1 - \nu^2)]$, bending stiffness
k_f $= \omega\{\omega^2 Eh^2/[12\rho(1 - \nu^2)r^4]\}^{-1/4}$, flexural wavenumber
k_{sn} modal wavenumbers for nth circumferential mode
m number of forces
M_x moment about the ϕ-axis
n number of circumferential modes
N_x axial force
$N_{x\phi}$ circumferential shear force
P_{co} controlled power transmission
P_e extensional wave power transmission
P_f flexural wave power transmission
P_s total power transmission
P_t torsional wave power transmission
P_{un} uncontrolled power transmission
P_{xa} active power transmission
P.T. power transmission
Q_x transverse shear
r cylinder mean radius
t time
T period of vibration
u axial displacement
v circumferential displacement
x_c control force location
x_e error sensor location
x_p primary force location
w flexural displacement
w_{c-f} flexural response due to unit control force excitation
w_{p-f} flexural response due to unit primary force excitation

α eigenroot coefficient
β eigenroot coefficient
γ^2 $=[\rho r^2(1-\nu^2)]/E$
θ_x angular rotation about the ϕ-axis
λ_f flexural wavelength
ν Poisson ratio
ξ $=h^2/12r^2$
ρ mass density
ϕ circumferential co-ordinate
ϕ_c phase of control force
ϕ_p phase of primary force
ω angular frequency of vibration

Superscripts

H complex conjugate and transpose of a matrix
T transpose of a matrix
$\dot{}$ derivative with respect to ϕ
$'$ derivative with respect to the dimensionless co-ordinate x/r,
* complex conjugate

Subscripts

c control force only
p primary force only